
Article:
Yu, Y, Cao, H, Wang, Z et al. (3 more authors) (2019) Texture-And-Shape Based Active Contour Model for Insulator Segmentation. IEEE Access, 7. pp. 78706-78714.

https://doi.org/10.1109/ACCESS.2019.2922257

IEEE Access
Multidisciplinary | Rapid Review | Open Access Journal

Date of publication xxxx 00, 0000, date of current version xxxx 00, 0000.

Digital Object Identifier 10.1109/ACCESS.2017.DOI

Texture-and-shape based active contour model for insulator segmentation

YAJIE YU[1], HUI CAO[1], ZHUZHU WANG[1],YUQIAO LI [1],KANG LI[2], and SHENGQUAN XIE[2]
[1]State Key Laboratory of Electrical Insulation and Power Equipment, School of Electrical Engineering, Xi'an Jiaotong University, Shaanxi Province, 710049, China
[2]School of Electronic and Electrical Engineering, University of Leeds, LS2 9JT, UK

This work is supported by Cooperation and Exchange Program of International Science and Technology of Shaanxi Province (2019KW-010) and Fundamental Research Funds for the Central University. Yajie Yu was supported by the China Scholarship Council for 1 year study at the University of Leeds.

ABSTRACT Insulator segmentation is a critical step for automatic insulator fault diagnosis in high voltage transmission systems. Existing methods fail to segment insulators when they have a low contrast with the surroundings. Considering the unique shape and texture characteristics of insulators, a texture-and-shape based active contour model is proposed for insulator segmentation. The segmentation is achieved by evolving a curve iteratively by the texture features and shape priors. In the texture-driven curve evolution, a semi-local region descriptor is used to extract the texture features of insulators and a new convex energy functional is defined based on the extracted features with the topology-preserving term. The topology-preserving term keeps the curve's topology unchanged as the curve topology is determined by the shape template. In the shape-driven curve evolution, the shape context descriptor is used to align the shape template with the current curve. The semantic transformation between the shape template and the current curve is obtained by Procrustes analysis and then adopted to update the current curve to resemble the shape prior. The proposed method is applied to a set of images, and the experimental results confirm the efficacy and effectiveness of the proposed method for segmenting insulators in cluttered backgrounds.

INDEX TERMS active contour model, insulator segmentation, level set, shape descriptor

I. INTRODUCTION

INsulators are critical equipment in high-voltage power transmission systems for electrical insulation and mechanical support. The insulator failures in a power system may lead to significant economic losses and even casualties [1], [2]. Therefore, monitoring the status of insulators is of great significance for power system safety. Traditional regular manual inspection is both time-consuming and power-consuming [3]–[5]. Insulator segmentation from the scene images is a prerequisite step for automatic fault diagnosis.

Insulator segmentation techniques can be roughly divided into two categories: patch-labeling methods and curve-evolution methods. In the patch-labeling methods, a patch may be just a pixel or a superpixel or a local region generated by a threshold, sliding window or clustering method. The features of these patches are then fed into a classifier to judge whether these patches belong to insulators [6]–[11]. The k-means clustering method is adopted to establish connected regions and then an adaptive neuro-fuzzy inference system is used to distinguish the insulator area [11]. The local directional pattern is used to classify the insulator regions by support vector machines [7]. A multi-scale and multi-feature descriptor is proposed to generate several spatial order features for insulator key point matching [8]. A six-layer convolution neural network is built to distinguish the insulator regions [9], [12]. A compact end-to-end neural network is trained by a two-stage training method in the framework of conditional generative adversarial networks for insulator segmentation [10], [13], [14]. There are two kinds of training samples, the roughly labelled position samples and the finely labelled segmented samples. These methods all need many labeled training samples to distinguish the insulators. Furthermore, it is hard to precisely extract insulators when they have low a contrast with the surroundings.

In the curve-evolution approach, often also referred to active contour models, some energy functional is defined to evolve a curve for insulator segmentation [11], [15]. The energy functional makes the curve-evolution methods an open framework that can incorporate external constraints flexibly [16], [17]. Gray Level Co-occurrence Matrix is employed

as the insulator texture descriptor in a global minimization active contour model [18]. A semi-local region descriptor is used in an active contour model to overcome the difficulties caused by the texture inhomogeneity [19]. Reference [20] uses the contourlet transformation for insulator texture analysis and then the fuzzy c-means is applied to cluster the insulator texture feature points to locate the initial curve. Chan-Vese model is finally used to detect the insulator boundaries. However, these methods fail to segment the insulators in the cluttered background where the insulator boundaries are difficult to distinguish.

Since insulators have a unique shape and texture, the shape constraint may be incorporated into a texture-based active contour model to capture insulator boundaries. A texture-and-shape based active contour model is thus proposed in this paper to segment insulators. A curve is evolved by the insulator texture features and shape priors alternatively to segment the insulator. In the texture-driven curve evolution, a semi-local region descriptor is used to extract the texture features of insulators in the Beltrami framework to overcome the difficulties caused by texture inhomogeneity [19], [21]. Based on the Chan-Vese model, a new convex energy functional is defined on the extracted texture features with the topology-preserving term. The length term and the area term of Chan-Vese model are omitted for the minimization of the length term and the area term is not necessary to drive the contour towards the boundary of the insulator and the information of length and area has already been considered in the shape-driven evolution. The topology-preserving term keeps the curve's topology unchanged since the curve topology is determined by the shape template [22]. In the numerical implementation, the addictive operator splitting scheme is adopted as it has a linear complexity and is easy to implement. In the shape-driven curve evolution, a shape is described by the distribution over relative position of the sampled points on a quantized log-polar coordinate. One-to-one point correspondences are built between the points from the shape template and the points from the current curve by minimizing a total matching cost to align the shape template with the current curve. The semantic transformation between the shape template and the current curve is obtained by Procrustes analysis and then adopted to update the current curve to resemble the shape prior. The method is applied to an insulator image dataset and the experimental results confirm that the proposed method is capable of segmenting the insulators in the cluttered background where the insulator boundaries are difficult to distinguish, outperforming other existing approaches.

The remainder of this paper is organized as follows. The related work is reviewed in Section II. A texture-and-shape based active contour model is proposed for insulator segmentation in Section III. A series of experiments are conducted on real life insulator images and the results are detailed in Section IV. Finally, Section V concludes the paper.

II. PRELIMINARIES

A. ACTIVE CONTOUR MODELS

Active contour models partition an image into sub-regions with continuous boundaries. Active contour models are classified into parametric active contours [23], [24] and geometric active contours [25]–[27] according to their representation and implementation. Parametric active contours are represented explicitly as parameterized curves in a Lagrangian formulation [28]. Geometric active contours are based on the level set theory and represented implicitly as the zero level set of a higher dimensional function [29]. The level set methods allow cusps, corners and automatic topological changes and make geometric active contours more flexible than parametric active contours [30]. Moreover, geometric active contours do not have to parameterize objects [31]. The image segmentation problem based on the level set methods can be formulated and solved by the well-established mathematical theories [32], [33]. The evolving contour C is embedded in a higher dimensional Lipschitz continuous function Φ and defined by $C = \{(x, y) | \Phi(x, y) = 0\}$. Evolving the curve C in the normal direction with speed F is equivalent to solving the following differential equation with the initial value Φ_0 [34]:

$$\frac{\partial \Phi}{\partial t} = |\nabla \Phi| F \tag{1}$$

Let Ω be the image domain, and $I : \Omega \to R$ be a gray level image. Mumford-Shah model approximates the image I by a piecewise smooth function Φ by minimizing the following energy functional [35]:

$$\begin{aligned} E^{MS}(\Phi, C) =& \mu Length(C) + \lambda \int_{\Omega} (I(\boldsymbol{x}) - \Phi(\boldsymbol{x}))^2 d\boldsymbol{x} \\ &+ \int_{\Omega \setminus C} |\nabla \Phi(\boldsymbol{x})|^2 d\boldsymbol{x} \end{aligned} \tag{2}$$

where C is the contour that segments the image into subregions and μ and λ are positive parameters. The length term is used to ensure regularity [36]. Mumford-Shah model is difficult to solve due to the nonconvexity of the functional.

Chan-Vese model can be regarded as a reduced form of Mumford-Shah model by restricting Φ as a piecewise constant function [15],

$$\Phi(\boldsymbol{x}) = \begin{cases} c_1 & \text{where is } \boldsymbol{x} \text{ inside } C, \\ c_2 & \text{where is } \boldsymbol{x} \text{ outside } C, \end{cases} \tag{3}$$

The energy functional of Chan-Vese model is defined as

$$\begin{aligned} E^{CV}(c_1, c_2, C) =& \lambda_1 \int_{inside(C)} (I(x) - c_1)^2 dx \\ &+ \lambda_2 \int_{outside(C)} (I(x) - c_2)^2 dx \\ &+ \mu Length(C) + \nu Area(inside(C)) \end{aligned} \tag{4}$$

where $\lambda_1, \lambda_1, \mu$ and ν are positive parameters. The area of the region inside C is added as an regularizing term. The image is approximated by the piecewise constant function Φ and is segmented into two subregions.

B. TEXTURE FEATURES IN THE BELTRAMI FRAMEWORK

A geometric way to represent images was proposed in the Beltrami frame where images can be considered as Riemannian manifolds embedded in a higher dimensional space [37]. For example, a 2-D gray image $I : R^2 \rightarrow R$ can be considered as a surface $\sum$ with local coordinates (x, y) embedded in R^3 by a mapping: $X : (x, y) \rightarrow (X_1 = x, X_2 = y, X_3 = I(x, y))$. This manifold-based representation of images has two main advantages. First, it allows the use of efficient differential geometry tools to perform various image processing tasks such as denoising or segmentation. Second, this framework works with arbitrary N dimensional images.

Reference [21] proposes a semi-local descriptor for image textures. The textures are represented by the intensity patch around the current pixel. The representation of textures in the Beltrami framework is given as follows:

$$X : (x, y) \rightarrow (X_1 = x, X_2 = y, X_3 = \mathcal{P}_{x,y}(I)) \quad (5)$$

where $\mathcal{P}_{x,y}$ is the square patch of size $\tau \times \tau$ around the pixel (x, y). The corresponding metric tensor g_{xy} of (6) is defined as:

$$g_{xy} = \begin{pmatrix} 1 + (\partial_x \mathcal{P}_{x,y})^2 & \partial_x \mathcal{P}_{x,y} \partial_y \mathcal{P}_{x,y} \\ \partial_x \mathcal{P}_{x,y} \partial_y \mathcal{P}_{x,y} & 1 + (\partial_y \mathcal{P}_{x,y})^2 \end{pmatrix} \quad (6)$$

Finally, the intrinsic texture descriptor is defined as follows:

$$F = e^{-\frac{\det(g_{xy})}{\sigma^2}} \quad (7)$$

where σ denotes a scaling parameter. The Gaussian kernel is adopted as a low-pass filter to control the degree of details. The semi-local operator can be extended to vector-valued images directly. Let $I = (I_1, I_2, \cdots, I_k)$ be a vector-valued image, where k denotes the number of channels. Then, the semi-local textures in the Beltrami framework are defined as:

$$\begin{aligned} X : (x, y) \rightarrow & (X_1 = x, X_2 = y, X_3 = \mathcal{P}_{x,y}(I_1), \\ & \cdots, X_{2+k} = \mathcal{P}_{x,y}(I_k)) \end{aligned} \quad (8)$$

The corresponding metric tensor g_{xy} of (6) is given as:

$$g_{xy} = \begin{pmatrix} 1 + \sum_{j=1}^{k} (\partial_x \mathcal{P}_{x,y})(I_j)^2 & \sum_{j=1}^{k} \partial_x \mathcal{P}_{x,y}(I_j) \partial_y \mathcal{P}_{x,y}(I_j) \\ \sum_{j=1}^{k} \partial_x \mathcal{P}_{x,y}(I_j) \partial_y \mathcal{P}_{x,y}(I_j) & 1 + \sum_{j=1}^{k} (\partial_y \mathcal{P}_{x,y})(I_j)^2 \end{pmatrix}$$

III. THE PROPOSED ALGORITHM

A texture-and-shape based active contour model for insulator segmentation is proposed in this paper. A curve is evolved by the insulator shape priors and texture features alternatively until the process converges or a fixed number of iterations is reached. The proposed method is detailed in the Algorithm 1.

Algorithm 1 The Proposed Model

Input: Image I to be segmented and insulator shape prior S;

Output: Final segmentation Φ^*

1: manually or automatically initialize the level set function Φ^0;
2: extract the texture feature map $F(I)$
3: **while** contour evolution is not converged or the fixed iterative time is not reached **do**
4: minimize the combined energy functional (9) to construct the intermediate level set function $\Phi^{n+\frac{1}{2}}$;
5: align the insulator shape prior S with the current contour $C^{n+\frac{1}{2}}$, namely, the zero level set of $\Phi^{n+\frac{1}{2}}$;
6: calculate the semantic shape transformation T and construct a new curve C^n and a new level set function Φ^{n+1};
7: **end while**

A. TEXTURE-DRIVEN CURVE EVOLUTION

The texture-driven curve evolution is realized by minimizing the energy functional defined on the texture features with the topology-preserving term. The energy functional is defined as follows:

$$\begin{aligned} E(c_1, c_2, C) = & \lambda [\int_{inside(C)} (F(\boldsymbol{x}) - c_1)^2 d\boldsymbol{x} \\ & + \int_{outside(C)} (F(\boldsymbol{x}) - c_2)^2 d\boldsymbol{x}] \\ & + E^T \end{aligned} \quad (9)$$

where $F(\bullet)$ represents the texture feature extraction operation and E^T denotes the topology-preserving term; c_1 and c_2 are the averages of $F(\boldsymbol{x})$ inside the contour and outside the contour, respectively; λ is the weighting parameter, $\lambda \geq 0$. The length term and the area term of the Chan-Vese model are omitted for two reasons. One is the information of length and area has already been considered in the shape-driven evolution. The other reason is that minimizing the length term and the area term does not necessarily drive the contour towards the boundary of the object. Although the ability of handling topological change is an advantage of the level set techniques, it is not necessary for insulator segmentation since the curve topology is determined by the shape priors.

For the level set formulation of our model, the contour C is represented by the zero level set of the Lipschitz funtion Φ and the variable C is replaced by Φ. The topology-preserving term was proposed based on a geometrical observation [22]. Consider two points $\boldsymbol{x}$ and $\boldsymbol{y}$ on the zero level line of Φ, and they are close enough to each other. $\nabla\Phi(\boldsymbol{x})$ and $\nabla\Phi(\boldsymbol{y})$ denote the unit outward normal vectors to the contour at $\boldsymbol{x}$ and $\boldsymbol{y}$. When the contour is about to merge or split, $\langle \nabla\Phi(\boldsymbol{x}), \nabla\Phi(\boldsymbol{y}) \rangle \simeq -1$. The topology-constraint term is

defined as follows:

$$E^T(\Phi) = -\iint_{\Omega\times\Omega} [e^{-\frac{\|\boldsymbol{x}-\boldsymbol{y}\|_2^2}{d^2}} \langle \nabla\Phi(\boldsymbol{x}), \nabla\Phi(\boldsymbol{y})\rangle \bullet W_l(\Phi(\boldsymbol{x})) W_l(\Phi(\boldsymbol{y}))] d\boldsymbol{x}d\boldsymbol{y} \quad (10)$$

where l denotes a level parameter, $\{\boldsymbol{x} \in \Omega \,|-l \le \Phi(\boldsymbol{x}) \le l\}$; $W_l(\Phi(\boldsymbol{x})) = H(\Phi(\boldsymbol{x}) + l) H(l - \Phi(\boldsymbol{x}))$ confines the points in a narrow band around the zero level line; $H(\bullet)$ represents the Heaviside function, defined as

$$H(z) = \begin{cases} 1 & \text{if } z \ge 0, \\ 0 & \text{if } z < 0, \end{cases} \quad (11)$$

$\langle \nabla\Phi(\boldsymbol{x}), \nabla\Phi(\boldsymbol{y})\rangle$ is weighted by the nearness of $\boldsymbol{x}$ and $\boldsymbol{y}$, $e^{-\frac{\|\boldsymbol{x}-\boldsymbol{y}\|_2^2}{d^2}}$. Therefore, the energy functional can be reformulated as follows:

$$\begin{aligned} E(c_1, c_2, \Phi) =& \lambda\{\int_\Omega [(F(\boldsymbol{x}) - c_1)^2 H(\Phi(\boldsymbol{x})) \\ &+ (F(\boldsymbol{x}) - c_2)^2 H(-\Phi(\boldsymbol{x}))] d\boldsymbol{x}\} \\ &- \iint_{\Omega\times\Omega} [e^{-\frac{\|\boldsymbol{x}-\boldsymbol{y}\|_2^2}{d^2}} \langle \nabla\Phi(\boldsymbol{x}), \nabla\Phi(\boldsymbol{y})\rangle \\ &\bullet W_l(\Phi(\boldsymbol{x})) W_l(\Phi(\boldsymbol{y}))] d\boldsymbol{x}d\boldsymbol{y} \end{aligned} \quad (12)$$

The minimization of (12) can be realized by solving by the following gradient flow equation

$$\frac{\partial\Phi}{\partial t} = -\frac{\partial E}{\partial\Phi} \quad (13)$$

The corresponding evolution equation could be deduced as

$$\begin{aligned} \frac{\partial\Phi}{\partial t} =& \lambda\delta(\Phi)\left[(F(\boldsymbol{x}) - c_2)^2 - (F(\boldsymbol{x}) - c_1)^2\right] \\ &+ \frac{4}{d^2} W_l(\Phi(\boldsymbol{x})) \int_\Omega e^{-\frac{\|\boldsymbol{x}-\boldsymbol{y}\|_2^2}{d^2}} (\boldsymbol{x} - \boldsymbol{y}) \\ &\bullet \nabla\Phi(\boldsymbol{y}) W_l(\Phi(\boldsymbol{y})) d\boldsymbol{y} \end{aligned} \quad (14)$$

In the numerical implementation, the addictive operator splitting scheme is adopted for it has linear complexity and is easy to implement [38], [39]. The addictive operator splitting scheme decomposes the 2-D problems into two 1-D subproblems . The discretization of (14) is

$$\begin{aligned} \Phi^{n+\frac{1}{2}} =& \frac{1}{2} \sum_{w\in\{x,y\}} B_w(\Phi(\boldsymbol{x})^n)^{-1} \{\Phi(\boldsymbol{x})^n + 4\frac{\tau}{d^2} W_l(\Phi(\boldsymbol{x})) \\ &\bullet \int_\Omega e^{-\frac{\|\boldsymbol{x}-\boldsymbol{y}\|_2^2}{d^2}} (\boldsymbol{x} - \boldsymbol{y}) \nabla\Phi(\boldsymbol{y}) W_l(\Phi(\boldsymbol{y})) d\boldsymbol{y} \\ &+ \tau\lambda[(F(\boldsymbol{x}) - c_1)^2 - (F(\boldsymbol{x}) - c_2)^2]\} \end{aligned} \quad (15)$$

where τ represents the timestep; $B_w(\Phi(\boldsymbol{x})^n) = Id - 2\tau A_w(\Phi(\boldsymbol{x})^n)$, $w \in \{x, y\}$. The entries of $A_w(\Phi(\boldsymbol{x})^n)$ is defined by

$$a_{ij_w} = \begin{cases} \frac{|\nabla\Phi_i^n|}{\frac{2}{(|\nabla\Phi_i^n| + |\nabla\Phi_j^n|)}} & \text{if } j \in N_w(i) \\ -|\nabla\Phi_i^n| \sum_{m\in N_w(i)} \frac{2}{(|\nabla\Phi_i^n| + |\nabla\Phi_m^n|)} & \text{if } j = i \\ 0 & \text{otherwise} \end{cases} \quad (16)$$

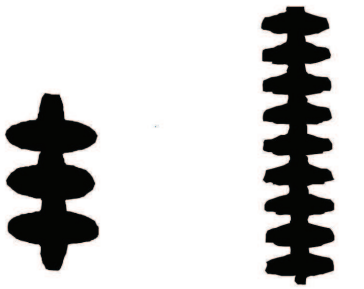

(a) Shape 1 (b) Shape 2

FIGURE 1. Insulator shape (a) Shape 1 (b) Shape 2

where w represents the directions, $w \in \{x, y\}$ and $N_w(i)$ represents the neighboring pixels of i in direction w. $B_w(\Phi(\boldsymbol{x})^n)$ is tridiagnonal, strictly diagonally dominant that can be solved efficiently by the Thomas algorithm. The smooth version of Heaviside function is used in the discretization stage, which is defined by

$$H_\varepsilon(z) = \frac{1}{2}\left(1 + \frac{2}{\pi}\arctan\left(\frac{z}{\pi}\right)\right) \quad (17)$$

B. SHAPE-DRIVEN CURVE EVOLUTION

Shape is an important factor to control the motion of the curve in insulator segmentation since insulators have the unique shape, as shown in Figure 1. The shape-driven curve evolution is realized by building a semantic transformation to make the evolving curve resemble the shape prior.

The shape context descriptor is used to align the shape template with the current curve and to calculate the semantic transformation [40], [41]. It is assumed that the shape of an object is essentially represented by a finite set of points sampled from the contour of the objects. These points do not need to correspond to key-points such as the maxima of a curvature. The shape context descriptor is generated by the distribution over relative positions of these sampled points. Given n points sampled from the shape contour, the shape context of a point p_i is defined by a histogram h_i:

$$h_i(k) = \#\{q \ne p_i : (q - p_i) \in bin(k)\} \quad (18)$$

h_i counts the number of the sampled neighbor points of p_i on a quantized log-polar coordinate that make the descriptor more sensitive to the nearby sampled points than to the points farther away.

As the shape context descriptor is represented by the distribution histograms, χ^2 test is used to measure the cost of matching two points. Given two points p_i and q_j, the matching cost is defined as the following:

$$C_{ij} \equiv C(p_i, q_j) = \frac{1}{2}\sum_{k=1}^{K} \frac{[h_i(k) - h_j(k)]}{h_i(k) - h_j(k)} \quad (19)$$

Consider two sets of points sampled from the shape template and the current contour, respectively. To align the shape

template with the current curve, one-to-one point correspondences are computed by minimizing the total matching cost [42],

$$H(\pi) = \sum_i C\left(p_i, q_{\pi(i)}\right) \tag{20}$$

where p_i represents a point on the current contour; $q_{\pi(i)}$ denotes a point on the shape template; π represents a permutation operator.

Procrustes analysis is adopted to estimate the transformation $T_{X_t,Y_t,s,\theta}$ from the current curve $C^{n+\frac{1}{2}}$ to the shape template S [43]. For a single point (x, y),

$$T_{X_t,Y_t,s,\theta}\begin{pmatrix} x \\ y \end{pmatrix} = \begin{pmatrix} s\cos\theta & s\sin\theta \\ -s\sin\theta & s\cos\theta \end{pmatrix}\begin{pmatrix} x \\ y \end{pmatrix} + \begin{pmatrix} X_t \\ Y_t \end{pmatrix},$$

where s is a scaling parameter, θ the rotation angle, (X_t, Y_t) the translation parameter. Given N correspondences of points, the transform parameters are obtained by minimizing the following equation (21):

$$J(T) = \sum_{i=1}^{N} \left|x_i - T_{X_t,Y_t,s,\theta}\left(x'_i\right)\right|^2 \tag{21}$$

,where x_i and x'_i denote the points of the shape template S and the corresponding points of the current contour $C^{n+\frac{1}{2}}$, respectively. The new curve C^n is represented by $\left\{T^{-1}{}_{X_t,Y_t,s,\theta}\left(x_1\right), \cdots, T^{-1}{}_{X_t,Y_t,s,\theta}\left(x_N\right)\right\}$ and used to construct a level set function Φ^n .

IV. EXPERIMENTAL RESULTS

To demonstrate the effectiveness of the proposed method, a series of experiments have been conducted on an insulator image dataset. The insulator image dataset consists of 100 arial images. Four methods are used to segment insulators, i.e. Chan-Vese model (CV) [15], Texture-based Chan-Vese model (T-CV) [19], Shape-based Chan-Vese model (S-CV) [17], Texture-and-shape-based Chan-Vese model (TS-CV). The segmentation error rate (ER) are adopted to evaluate these segmentation methods. ER is defined as the ratio of misclassified image pixels over the total image pixels. The test platform of the algorithm used Windows 7 Ultimate, the configuration of test PC is 1.87 GHz frequency with 6 GB memory, and the algorithms are performed in MATLAB R2015a.

In the experiments, three types of contours are used to initialize the level set function, i.e. a rectangular, a small circle and a big circle. In the numerical implementation, the weighting parameter λ is set to 1; the topology-preserving term parameters d and l are set to 4 and 1, respectively, according to [44]; the timestep τ is empirically chosen in the range of [0.1,1] in step of 0.1 and is set to 0.1.

The insulator image 1 and its texture image are shown in Figure 2. Figure 1a is used as the insulator shape prior. Figure 2 shows the process of the proposed method. The insulator segmentation is achieved by texture-driven curve evolution and shape-driven curve evolution alternatively. A rectangle is used to initialize the level set function. The second column shows the intermediate curves $C^{n+\frac{1}{2}}$ by minimizing the equation (9). The curves are aligned with the insulator template by finding point correspondences, as shown in the third column. Then the curves are updated by the semantic transform from the intermediate curves to the shape template. The forth column shows the contours C^n after the shape-driven curve evolution. The process reveals the areas of texture similarity could be segmented by the texture-driven curve evolution and the shape prior could help to segment the insulators from the similar texture regions.

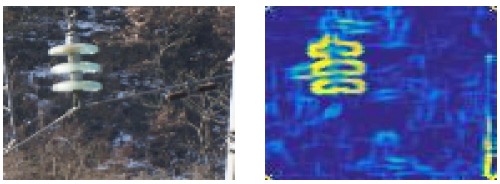

(a) original image (b) texture image

FIGURE 2. Insulator image 1 (a) original image (b) texture image.

The segmentation results of image 1 are shown in Figure 4. Figure 4a shows the initial contours. Figure 4b illustrates the segmentation results of CV. The insulator is segmented but the grass is also segmented as part of the insulator. Figure 4c shows the segmentation results of T-CV and most of the grass is eliminated. Figure 4d and Figure 4e show the segmentation results of S-CV and TS-CV, respectively and insulators are accurately segmented from the original image 1 by S-CV and TS-CV. The segmentation results show that the texture features and the shape prior can improve the segmentation results and the initial contours have no influence on the final results. Comparing Figure 4c to Figure 4d, we can conclude that the shape is a very effective characteristic for insulator segmentation.

The insulator image 2 and its texture feature are shown in Figure 5. Figure 1b is used as the shape prior. The segmentation results are shown in Figure 6. Figure 6a shows the initial contours and Figure 6 b∼e shows the segmentation results of CV, T-CV, S-CV and TS-CV, respectively. For the insulator image 2, the segmentation results of CV also contains many background objects. The segmentation results of T-CV contains less background but still unsatisfactory. S-CV and TS-CV both achieve satisfactory results.

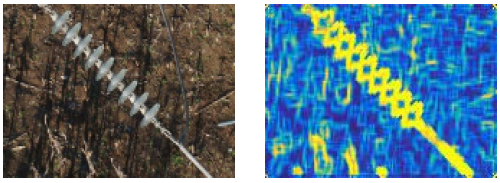

(a) original image (b) texture image

FIGURE 5. Insulator image 2 (a) original image (b) texture image.

Figure 7 shows the insulator image 3 and its texture feature. The background of the insulator image 3 is more complex and the insulator has low contrast with the surroundings.

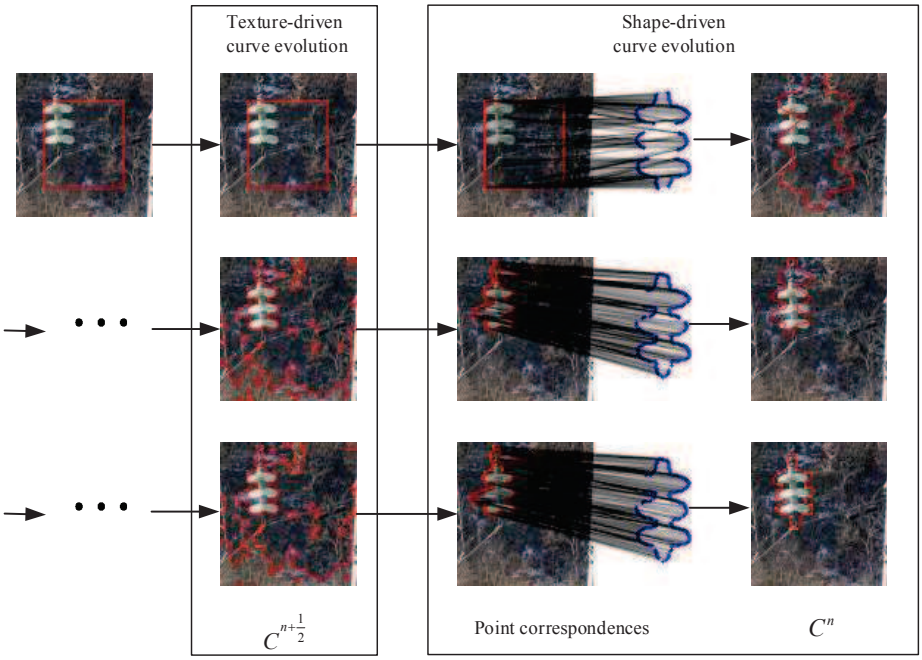

FIGURE 3. The process of the proposed method.

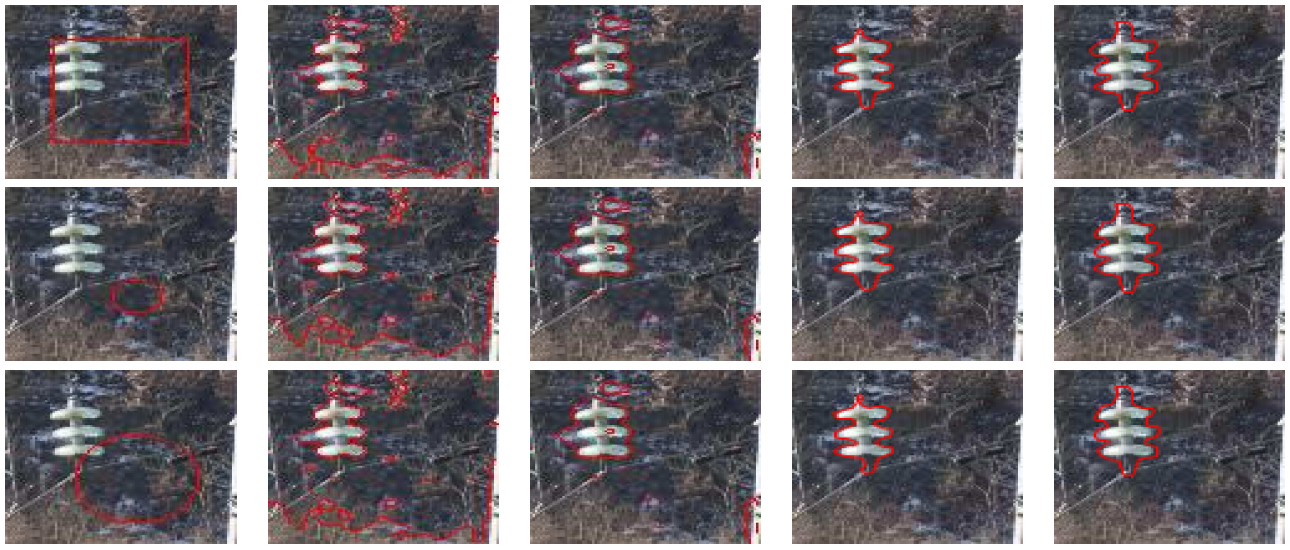

FIGURE 4. Insulator segmentation results for image 1 (a)initial contour (b)CV (c)T-CV (d)S-CV (e)TS-CV.

Figure 1b is used as the shape prior and the segmentation results are shown in Figure 7. Figure 8a shows the initial contours and Figure 8 b∼e illustrate the segmentation results of CV, T-CV, S-CV and TS-CV, respectively. Figure 8b, 8c and 8d reveal that CV, T-CV and S-CV fail to drive the contour to approximate the boundaries of the insulator. The proposed method is capable of distinguishing the insulator boundaries as shown in Figure 8e. The segmentation results also show that the initial contours have no influence on the final segmentation result.

The computational time and ER of these four methods

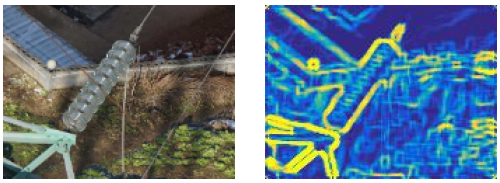

FIGURE 7. Insulator image 1 (a) original image (b) texture image.

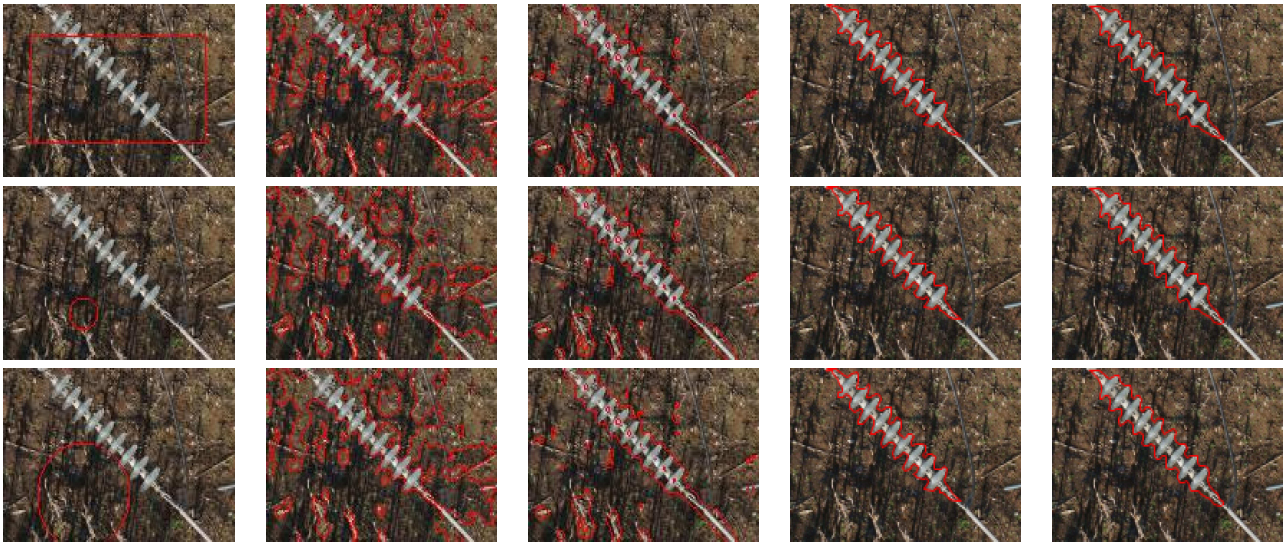

FIGURE 6. Insulator segmentation results for image 2 (a)initial contour (b)CV (c)T-CV (d)S-CV (e)TS-CV.

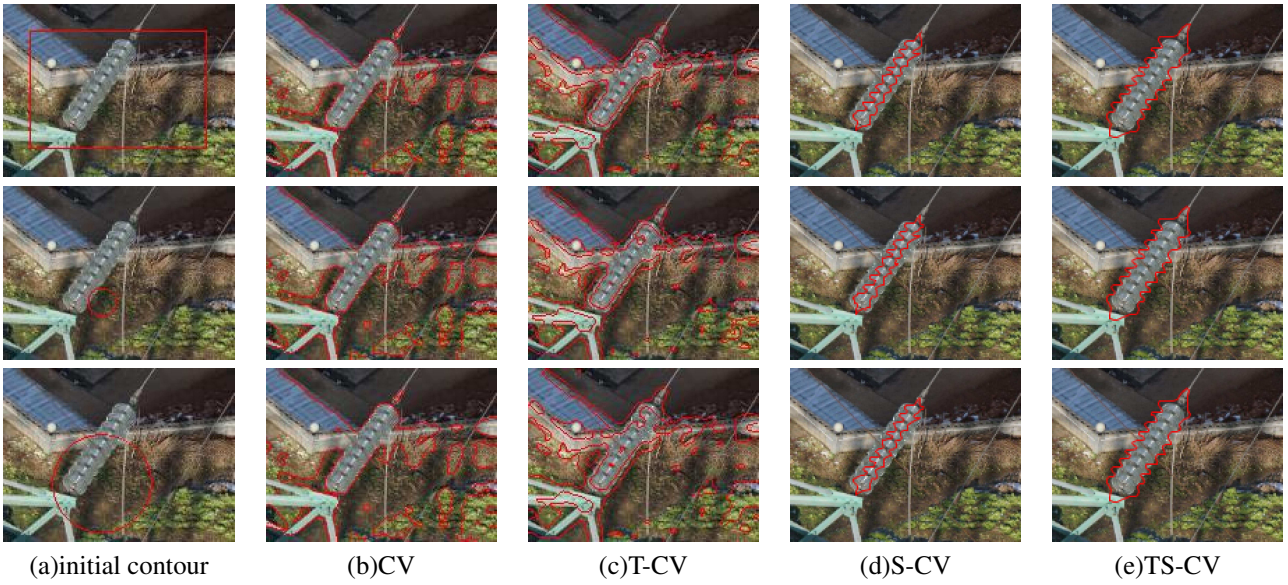

FIGURE 8. Insulator segmentation results for image 3 (a)initial contour (b)CV (c)T-CV (d)S-CV (e)TS-CV.

TABLE 1. Comparison of the computational time

Method	CV	T-CV	S-CV	TS-CV
Time(s)	1.15	2.01	10.14	10.99
ER(%)	33.21	20.79	8.45	4.39

are listed in Table 1. Although TS-CV achieves the best segmentation results, it is the most time-consuming method. Compared the computational time of CV with T-CV and S-CV, we can conclude that the shape-driven curve evolution approach however would take much more time.

V. CONCLUSION

In the paper, a texture-and-shape based active contour model is proposed for segmenting insulators in the cluttered background. Shape constraint is incorporated into a texture-based active contour model to capture the insulator boundaries. The experiments on the insulator image dataset confirm that the proposed method can segment the insulators in the cluttered background where the boundaries of insulators are difficult to be distinguished and it outperforms other related methods. As the shape-driven curve evolution process is time-consuming, future work will focus on speeding up the shape-driven curve evolution process and extending the proposed method for real-time detection applications.

REFERENCES

[1] X. Miao, X. Liu, J. Chen, S. Zhuang, J. Fan, and H. Jiang, "Insulator detection in aerial images for transmission line inspection using single shot multibox detector," IEEE Access, 2019.

[2] X. Tao, D. Zhang, Z. Wang, X. Liu, H. Zhang, and D. Xu, "Detection of power line insulator defects using aerial images analyzed with convolutional neural networks," IEEE Transactions on Systems, Man, and Cybernetics: Systems, 2018.
[3] W. Chang, G. Yang, Z. Wu, and Z. Liang, "Learning insulators segmentation from synthetic samples," in 2018 International Joint Conference on Neural Networks (IJCNN). IEEE, 2018, pp. 1–7.
[4] H. Lu, Y. Li, S. Mu, D. Wang, H. Kim, and S. Serikawa, "Motor anomaly detection for unmanned aerial vehicles using reinforcement learning," IEEE internet of things journal, vol. 5, no. 4, pp. 2315–2322, 2018.
[5] S. Serikawa and H. Lu, "Underwater image dehazing using joint trilateral filter," Computers & Electrical Engineering, vol. 40, no. 1, pp. 41–50, 2014.
[6] Z. Zhao, X. Fan, G. Xu, L. Zhang, Y. Qi, and K. Zhang, "Aggregating deep convolutional feature maps for insulator detection in infrared images," IEEE Access, vol. 5, pp. 21 831–21 839, 2017.
[7] T. Jabid and M. Z. Uddin, "Rotation invariant power line insulator detection using local directional pattern and support vector machine," in 2016 International Conference on Innovations in Science, Engineering and Technology (ICISET). IEEE, 2016, pp. 1–4.
[8] S. Liao and J. An, "A robust insulator detection algorithm based on local features and spatial orders for aerial images," IEEE Geoscience and Remote Sensing Letters, vol. 12, no. 5, pp. 963–967, 2015.
[9] Y. Liu, J. Yong, L. Liu, J. Zhao, and Z. Li, "The method of insulator recognition based on deep learning," in 2016 4th International Conference on Applied Robotics for the Power Industry (CARPI). IEEE, 2016, pp. 1–5.
[10] W. Chang, G. Yang, J. Yu, and Z. Liang, "Real-time segmentation of various insulators using generative adversarial networks," IET Computer Vision, vol. 12, no. 5, pp. 596–602, 2018.
[11] M. J. B. Reddy, B. K. Chandra, and D. Mohanta, "A DOST based approach for the condition monitoring of 11 kV distribution line insulators," IEEE Transactions on Dielectrics and Electrical Insulation, vol. 18, no. 2, pp. 588–595, 2011.
[12] H. Lu, Y. Li, M. Chen, H. Kim, and S. Serikawa, "Brain intelligence: go beyond artificial intelligence," Mobile Networks and Applications, vol. 23, no. 2, pp. 368–375, 2018.
[13] H. Lu, D. Wang, Y. Li, J. Li, X. Li, H. Kim, S. Serikawa, and I. Humar, "Conet: A cognitive ocean network," arXiv preprint arXiv:1901.06253, 2019.
[14] H. Lu, Y. Li, T. Uemura, H. Kim, and S. Serikawa, "Low illumination underwater light field images reconstruction using deep convolutional neural networks," Future Generation Computer Systems, vol. 82, pp. 142–148, 2018.
[15] T. F. Chan and L. A. Vese, "Active contours without edges," IEEE Transactions on image processing, vol. 10, no. 2, pp. 266–277, 2001.
[16] X. Shan, X. Gong, and A. K. Nandi, "Active contour model based on local intensity fitting energy for image segmentation and bias estimation," IEEE Access, vol. 6, pp. 49 817–49 827, 2018.
[17] B. Wang, X. Yuan, X. Gao, X. Li, and D. Tao, "A hybrid level set with semantic shape constraint for object segmentation," IEEE transactions on cybernetics, no. 99, pp. 1–2, 2018.
[18] Q. Wu, J. An, and B. Lin, "A texture segmentation algorithm based on PCA and global minimization active contour model for aerial insulator images," IEEE Journal of Selected Topics in Applied Earth Observations and Remote Sensing, vol. 5, no. 5, pp. 1509–1518, 2012.
[19] Q. Wu and J. An, "An active contour model based on texture distribution for extracting inhomogeneous insulators from aerial images," IEEE Transactions on Geoscience and Remote Sensing, vol. 52, no. 6, pp. 3613–3626, 2014.
[20] G. Zhang, Z. Liu, and Y. Han, "Automatic recognition for catenary insulators of high-speed railway based on contourlet transform and Chan–Vese model," Optik, vol. 127, no. 1, pp. 215–221, 2016.
[21] N. Houhou, J.-P. Thiran, and X. Bresson, "Fast texture segmentation based on semi-local region descriptor and active contour," Numerical Mathematics: Theory, Methods and Applications., vol. 2, no. ARTICLE, 2009.
[22] C. Le Guyader and L. A. Vese, "Self-repelling snakes for topology-preserving segmentation models," IEEE Transactions on Image Processing, vol. 17, no. 5, pp. 767–779, 2008.
[23] M. Kass, A. Witkin, and D. Terzopoulos, "Snakes: Active contour models," International journal of computer vision, vol. 1, no. 4, pp. 321–331, 1988.
[24] L. D. Cohen, "On active contour models and balloons," CVGIP: Image understanding, vol. 53, no. 2, pp. 211–218, 1991.
[25] V. Caselles, F. Catté, T. Coll, and F. Dibos, "A geometric model for active contours in image processing," Numerische mathematik, vol. 66, no. 1, pp. 1–31, 1993.
[26] V. Caselles, R. Kimmel, and G. Sapiro, "Geodesic active contours," in Proceedings of IEEE international conference on computer vision. IEEE, 1995, pp. 694–699.
[27] A. Yezzi, S. Kichenassamy, A. Kumar, P. Olver, and A. Tannenbaum, "A geometric snake model for segmentation of medical imagery," IEEE Transactions on medical imaging, vol. 16, no. 2, pp. 199–209, 1997.
[28] D. Terzopoulos and K. Fleischer, "Deformable models," The visual computer, vol. 4, no. 6, pp. 306–331, 1988.
[29] S. Osher and R. Fedkiw, Level set methods and dynamic implicit surfaces. Springer Science & Business Media, 2006, vol. 153.
[30] C. Xu, A. Yezzi, and J. L. Prince, "On the relationship between parametric and geometric active contours," in Conference Record of the Thirty-Fourth Asilomar Conference on Signals, Systems and Computers (Cat. No. 00CH37154), vol. 1. IEEE, 2000, pp. 483–489.
[31] C. Li, R. Huang, Z. Ding, J. C. Gatenby, D. N. Metaxas, and J. C. Gore, "A level set method for image segmentation in the presence of intensity inhomogeneities with application to mri," IEEE transactions on image processing, vol. 20, no. 7, pp. 2007–2016, 2011.
[32] R. MALLADI, "Shape modeling with front propagation: A level set approach," IEEE Trans. PAMI, vol. 17, no. 2, pp. 158–175, 1995.
[33] G. Aubert and P. Kornprobst, Mathematical problems in image processing: partial differential equations and the calculus of variations. Springer Science & Business Media, 2006, vol. 147.
[34] S. Osher and J. A. Sethian, "Fronts propagating with curvature-dependent speed: algorithms based on hamilton-jacobi formulations," Journal of computational physics, vol. 79, no. 1, pp. 12–49, 1988.
[35] D. Mumford and J. Shah, "Optimal approximations by piecewise smooth functions and associated variational problems," Communications on pure and applied mathematics, vol. 42, no. 5, pp. 577–685, 1989.
[36] P. Getreuer, "Chan-vese segmentation," Image Processing On Line, vol. 2, pp. 214–224, 2012.
[37] N. Sochen, R. Kimmel, and R. Malladi, "A general framework for low level vision," IEEE transactions on image processing, vol. 7, no. 3, pp. 310–318, 1998.
[38] J. Weickert, B. Romeny, M. A. Viergever et al., "Efficient and reliable schemes for nonlinear diffusion filtering," IEEE transactions on image processing, vol. 7, no. 3, pp. 398–410, 1998.
[39] J. Weickert and G. Kühne, "Fast methods for implicit active contour models," in Geometric level set methods in imaging, vision, and graphics. Springer, 2003, pp. 43–57.
[40] T. H. N. Le and M. Savvides, "A novel shape constrained feature-based active contour model for lips/mouth segmentation in the wild," Pattern Recognition, vol. 54, pp. 23–33, 2016.
[41] S. Belongie, J. Malik, and J. Puzicha, "Shape matching and object recognition using shape contexts," IEEE Transactions on Pattern Analysis & Machine Intelligence, no. 4, pp. 509–522, 2002.
[42] R. Jonker and A. Volgenant, "A shortest augmenting path algorithm for dense and sparse linear assignment problems," Computing, vol. 38, no. 4, pp. 325–340, 1987.
[43] D. G. Kendall, "A survey of the statistical theory of shape," Statistical Science, pp. 87–99, 1989.
[44] H. Schaeffer, N. Duggan, C. l. Guyader, and L. Vese, "Topology preserving active contours," Communications in Mathematical Sciences, vol. 12, no. 7, pp. 1329–1342, 2014.